Journal of Polytechnic, 2016; 19 (4) : 593-602

# Deformation and Electrical Behaviours of Functionally Graded Piezoelectric Curved Sensors

**Eray ARSLAN**

Department of Mechanical Engineering, Inonu University, Malatya, Turkey

( Received :03.05.2016 ; Accepted : 17.06.2016 )

**ABSTRACT**

A comprehensive analytical model is developed for a functionally graded piezoelectric (FGP) curved bar which is in a closed electrical circuit. Piezoelectric coefficient is assumed to vary in the radial direction according to a power law unlike the corresponding studies in the literature. This assumption constitutes one of the basic novelties of the present investigation. For the verification, the numerical results of the mathematical model for an FGP curved actuator are compared with those of a related study on a linear FGP curved bar in the literature. Next, the model is used to determine the deformation and electrical behaviours of an FGP curved sensor under a couple at its free end section. The presentation of the numerical results for the curved sensors is another novelty of the present study since the numerical results in the related studies in the literature were presented just for the actuators. Results are compared with bimorph piezoelectric curved sensors and the effect of the grading parameter on the mechanical and electrical fields is examined. Numerical results show that FGP curved sensor provides several advantages in terms of the mechanical behavior of the material, and the distribution and production of electric potential in the sensor are affected significantly with the variation of grading parameter.

**Keywords: Piezoelectric materials, functionally graded curved sensor and actuator, analytical model, bending moment.**

**ÖZ**

Kapalı elektrik çevrimi içerisinde bulunan fonksiyonel derecelendirilmiş piezoelektrik (FDP) eğri eksenli kiriş için kapsamlı bir analitik model geliştirilmiştir. Literatürdeki ilgili çalışmaların aksine, piezoelektrik sabitinin radyal doğrultuda bir güç yasasına bağlı olarak değiştiği kabul edilmiştir. Bu kabul, çalışmanın temel orijinalitesinden birini oluşturmaktadır. FDP eğri eksenli bir eyleyici için modelin sayısal sonuçları, literatürdeki ilgili çalışmalar ile karşılaştırılarak, modelin sınanması sağlanmıştır. Ardından, model serbest ucundan eğilme momentine mağruz bırakılan FDP eğri eksenli sensörün mekanik ve elektrik alanını elde etmek için kullanılmıştır. Literatürdeki diğer çalışmalarda sadece eyleyiciler için sonuçlar sunulduğundan dolayı, sensör için sayısal sonuçların sunumu bu çalışmanın bir diğer orijinalliğini temsil etmektedir. Sonuçlar iki tabakalı (bimorph) piezoelektrik eğri eksenli sensör sonuçları ile karşılaştırılmış ve derecelendirme parametresinin mekanik ve elektrik alanındaki etkileri incelenmiştir. Sonuçlar göstermiştir ki, FDP eğri eksenli sensör, malzemenin mekanik davranışları açısından bir çok avantaj sergilemektedir. Elektrik potensiyelinin dağılımı ve üretimi ise derecelendirme parametresine bağlı olarak önemli ölçüde etkilenmiştir.

**Anahtar Kelimeler: Piezoelektrik malzeme, fonksiyonel derecelendirilmiş eğri eksenli sensör ve eyleyici, analitik model, eğilme momenti.**

## 1. INTRODUCTION

Piezoelectric materials are found frequently in many smart structures such as actuators and sensors to realize conversions between mechanical and electrical fields [1-3]. Generating electric potential in a piezoelectric material which works under a mechanical load is known as reversible "sensor" behavior (direct effect). On the other hand, piezoelectric material is called as an "actuator" when an initial electric potential, which causes displacement, is applied onto the structure (converse effect) [1]. In general, the material may be set on a flat [4-6] or circular bar or panel [3,7-11] depending of the purpose of its use. At this point, the geometry of the piezoelectric sensor and/or actuator should be selected according to the shape of the surface on which it is settled. When a flat piezoelectric material is bonded onto structures with complex curved shapes, its sensitivity decreases [4,12]. In these cases, curved sensors or actuators have more advantages than flat piezoelectric materials, particularly in providing precise information at a test point [13,14]. Moreover, totally different deformation and electrical behaviors are exhibited by flat and curved materials under the same type of loading. For example, there is no stress component in a linearly graded flat actuator subjected to an external electrical load [15], whereas some non-zero stress components emerge in a curved actuator under the same loading condition [16]. Hence, detailed researches must be examined to determine the behaviors of the piezoelectric curved sensors and actuators separately [16].

There are several studies in which mechanical and electrical behaviors of unimorph [17,18], bimorph [19-22], and multimorph [23-26] flat sensors and actuators have been investigated. In these investigations, it is considered that the actuators are subjected to an electric field while the sensors are under harmonic excitations, static shear force, axial force or bending moment. Moreover, mathematical models to define the mechanical behavior have also been developed for functionally graded piezoelectric (FGP) flat sensors [27-30] and actuators [15,31-35]. Indeed, the general use of a

*Corresponding Author
e-mail: eray.arslan@inonu.edu.tr
Digital Object Identifier (DOI) : 10.2339/2016.19.4 531-535

Functionally Graded Material (FGM) provided several advantages to different fields of engineering in terms of device performance related to strength [36], weight [37], electricity production [32], and so forth [38]. It is recalled that the material properties in a structure with FGM vary continuously, and therefore it should be tailored in order to meet different requirements [37]. In the piezoelectric applications, the functionally graded structures are used to reduce the stress concentration at the interface surfaces which exist in the bimorph and multimorph (even in unimorph [39]) piezoelectric materials while maintaining high bending displacement [32]. In these structures, stress discontinuity can be significantly reduced [31], which improves the reliability of the structures [25]. Hence, as mentioned above, a number of investigations have so far been conducted on FGP with flat sensors and actuators.

Circular curved actuators are considered in some other investigations. Kuang et. al. [40] investigated the effect of parameters on the static response of curved unimorph and bimorph actuators under an input voltage. Zhou et. al. [41] presented an analytical model for a multilayered piezoelectric curved bar subjected to mechanical loads. Dynamic analysis of an FGP curved bar was performed by Su et. al. for different boundary conditions [42]. Analytical models were presented by Shi [16] to demonstrate the bending behavior of bimorph and graded curved piezoelectric actuators. In the study, the researcher assumed that the actuators are poled in the radial direction and they are subjected to electric potential between the inner and outer cylindrical surfaces. In the FGP curved actuator model, it was considered that piezoelectric coefficient varies linearly in the radial direction while other material coefficients are assumed to be constant. Shi and Zhang [33] followed a similar analysis but they assumed that the piezoelectric coefficients vary according to a Taylor series expansion for a curved actuator. The same problem but for a multilayered piezoelectric curved actuator was solved by Zhang and Shi [13]. In the same study, they also derived an exact solution for a FGP curved actuator in which nonlinear distribution of the piezoelectric coefficient is assumed to vary according to second order polynomial. The study conducted by Arslan and Usta [43] can be taken as an example of an analysis on the behavior of a piezoelectric curved sensor. In the study, the researchers presented a mathematical model based on the theory of elasticity and is developed for a piezoelectric bimorph curved sensor subjected to pure bending. To sum up, in the literature, there are several studies in which exact solutions are presented for FGP actuators but not for a sensor. There is no previously reported study in the literature on an adequate analytical solution for an FGP curved sensor under mechanical loads. Hence, the aim of the present work is to investigate the mechanical and electrical behaviors of such a curved sensor subjected to a couple, which provides pure bending conditions. At this point, the novelty of the present investigation can listed as follows:

- More comprehensive analytical model than the related studies in the literature [13,33] is presented,
- Piezoelectric coefficient is assumed to vary in the radial direction according to a power law unlike the corresponding studies in the literature [13,16,33],
- Numerical results are presented not only for the curved actuators but also for the sensors.

In this study, in other words, a general analytical model (which is more comprehensive than Shi's linear one [16]) for a nonlinearly FGP curved bar is developed. Moreover, numerical results for a nonlinearly FGP curved sensor under a mechanical load are presented. It is assumed that the piezoelectric coefficient varies in radial direction nonlinearly according to a power law but other mechanical and electrical coefficients remain constant in the whole bar. The basic assumptions and equations are based on theory of elasticity for a cylindrical coordinate system. They are used to derive the analytical expressions for the stresses, displacements and electric potential [36, 43-45]. The model is first solved for an FGP actuator in which a closed circuit voltage is subjected to its outer cylindrical surface and the numerical responses are compared with those of Shi's linear FGP model [16] after selecting the appropriate grading parameter. Then, the mechanical and electrical fields of an FGP curved sensor subjected to a couple at its free end section are obtained by using the model. The effects of the grading parameter on displacements, stresses, and electric potential are presented and advantages of FGP sensor (over bimorph one [43]) are discussed.

## 2. BASIC EQUATIONS

The geometry of the functionally graded piezoelectric curved bar which is in a closed electrical circuit [20] (and the coordinate system used) is presented in Fig 1. The direction of the polarization (in the radial direction $r$) is also shown with an arrow in Fig. 1 [46]. The bar is subjected to a couple $M$ at the end where $\theta = 0$ (and for $r_{in} \leq r \leq r_{out}$) and it is fixed at the other end ($\theta = \pi/2$). A state of plane stress (axial stress component $\sigma_z$ vanishes) and small deformations are presumed. Assumption of the cylindrical symmetry is considered. Hence, only the components of displacement in radial $u$ and circumferential $v$ directions are functions of both radial coordinate $r$ and the circumferential coordinate $\theta$. However, the other quantities are only a function of $r$. Moreover, the such assumption provides that the shear stress $\tau_{r\theta}$, the shear strain $\gamma_{r\theta}$, the circumferential component of electric displacement vector $D_\theta$, and circumferential electric field $E_\theta$ vanish.

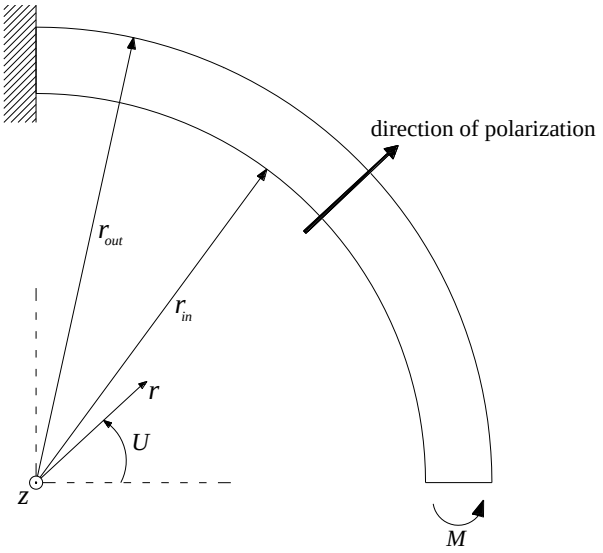


**Figure 1.** Piezoelectric FGP curved bar.

Taking a variable piezoelectric coefficient $g_{31} = g_{31}(r)$, the governing constitutive equations read

$$\varepsilon_\theta = S_{11}\sigma_\theta + S_{13}\sigma_r + g_{31}(r)D_r, \quad (1)$$

$$\varepsilon_r = S_{13}\sigma_\theta + S_{33}\sigma_r + g_{33}D_r, \quad (2)$$

$$E_r = -g_{31}(r)\sigma_\theta - g_{33}\sigma_r + \zeta_{33}D_r \quad (3)$$

where $\varepsilon_i$ denote strains, $\sigma_i$-stresses, $D_r$-radial electric displacement vector, $S_{ij}$-the components of the effective elastic compliance, $g_{31}(r)$ and $g_{33}$-the piezoelectric coefficients (Type-g), and $\zeta_{33}$ - the dielectric permittivity coefficient. Here it is noted that the piezoelectric coefficient $g_{31}(r)$ is assumed to vary in the radial direction according to a power law [37]

$$g_{31}(r) = A\left(\frac{r}{r_{in}}\right)^n + B \quad (4)$$

where $n$ is the grading parameter of the material, $A$ and $B$ are constants, and $r_{in}$ is the inner surface radius of the bar (see Fig. 1). While this material property depends on the radial coordinate, other material coefficients (i.e. $S_{11}$, $S_{13}$, $S_{33}$, $g_{33}$, $\zeta_{33}$ are however assumed to be constant in the whole bar since the dependence of $g_{31}$ on the degree of polling is higher than those of the remaining coefficients [28]. The strain-displacement relations are

$$\varepsilon_r = \frac{\partial u}{\partial r}, \quad (5)$$

$$\varepsilon_\theta = \frac{u}{r} + \frac{1}{r}\frac{\partial v}{\partial \theta}, \quad (6)$$

$$\gamma_{r\theta} = \frac{1}{r}\frac{\partial u}{\partial \theta} + \frac{\partial v}{\partial r} - \frac{v}{r} = 0. \quad (7)$$

The relationship between electric potential $\phi$ and radial electric field $E_r$ provides

$$E_r = -\frac{d\phi}{dr}. \quad (8)$$

The compatibility equation is

$$\frac{d^2\varepsilon_\theta}{dr^2} + \frac{2}{r}\frac{d\varepsilon_\theta}{dr} - \frac{1}{r}\frac{d\varepsilon_r}{dr} = 0. \quad (9)$$

Integration of the compatibility relation (9) by parts gives [45]

$$\frac{d}{dr}(r\varepsilon_\theta) - \varepsilon_r = C_2 \quad (10)$$

where $C_2$ is an arbitrary integration constant. The equations of equilibrium for the principle stresses (in the absence of body force) and electric displacement vectors (for no body charge) read

$$\frac{d(r\sigma_r)}{dr} - \sigma_\theta = 0, \quad (11)$$

$$\frac{1}{r}\frac{d}{dr}(rD_r) = 0. \quad (12)$$

## 3. GOVERNING EQUATIONS

Solution of Eq. (12) simply is

$$D_r = \frac{C_1}{r} \quad (13)$$

where $C_1$ is a constant of integration. Using Eq. (11) and substituting Eqs. (1), (2), and (13) into Eq. (10) yield a differential equation for the radial stress

$$r^2 S_{11}\frac{d^2\sigma_r}{dr^2} + 3rS_{11}\frac{d\sigma_r}{dr} + (S_{11} - S_{33})\sigma_r = C_1\left[\frac{g_{33}}{r} - \frac{An\left(\frac{r}{r_{in}}\right)^{-1+n}}{r_{in}}\right] + C_2, \quad (14)$$

with the solution

$$\sigma_r = -\frac{C_1}{r}\left[\frac{An\left(\frac{r}{r_{in}}\right)^n}{n^2S_{11} - S_{33}} + \frac{g_{33}}{S_{33}}\right] + \frac{C_2}{S_{11} - S_{33}} + C_3 r^{-1-S} + C_4 r^{-1+S} \quad (15)$$

where $C_3$ and $C_4$ are new integration constants and

$$S = \sqrt{\frac{S_{33}}{S_{11}}}. \quad (16)$$

From Eq. (11), one obtains for the circumferential stress component the expression

$$\sigma_\theta = -\frac{AC_1 n^2\left(\frac{r}{r_{in}}\right)^n}{r(n^2S_{11} - S_{33})} + \frac{C_2}{S_{11} - S_{33}} - C_3 S r^{-1-S} + C_4 S r^{-1+S}. \quad (17)$$

Eqs. (8), (13), (15), and (17) are inserted in Eq. (3) and then solved:

$$\phi(r) = -C_1\left\{\frac{A\left(\frac{r}{r_{in}}\right)^n\left\{2g_{33} + n\left[2B + A\left(\frac{r}{r_{in}}\right)^n\right]\right\}}{2(n^2S_{11} - S_{33})} + \frac{(g_{33}^2 + S_{33}\zeta_{33})lnr}{S_{33}}\right\} + \frac{C_2 r\left[(1+n)(B+g_{33}) + A\left(\frac{r}{r_{in}}\right)^n\right]}{(1+n)(S_{11} - S_{33})} - \frac{C_3 r^{-S}}{S}\left\{g_{33} - S\left[B - \frac{A\left(\frac{r}{r_{in}}\right)^n S}{n-S}\right]\right\} + \frac{C_4 r^S}{S}\left\{g_{33} + S\left[B + \frac{A\left(\frac{r}{r_{in}}\right)^n S}{n+S}\right]\right\} + C_5. \quad (18)$$

Here, a new integration constant $C_5$ is introduced. To determine radial and circumferential displacement components, the formulation in [44] has been followed.

If the expressions above is substituted into Eq. (5) and integrated for $r$, following equation is obtained

$$u(r,\theta) = -\frac{C_1 A\left(\frac{r}{r_{in}}\right)^n (nS_{13}+S_{33})}{n^2 S_{11}-S_{33}} + \frac{C_2 r(S_{13}+S_{33})}{S_{11}-S_{33}} + \frac{C_3 r^{-S}(S\,S_{13}-S_{33})}{S} + \frac{C_4 r^{S}(S\,S_{13}+S_{33})}{S} + f_1(\theta) \quad (19)$$

where $f_1$ is a function of circumferential direction $\theta$, only. On the other hand, Eq. (6) can be expressed as

$$\frac{\partial v}{\partial \theta} = \varepsilon_\theta r - u. \quad (20)$$

Substituting Eqs. (1) and (19) into Eq. (20) and integrating it for $\theta$ give

$$v(r,\theta) = \left[C_1\left(B - \frac{g_{33}S_{13}}{S_{33}}\right) + C_2 r - \frac{r^{-S}(C_3 - C_4 r^{2S})(S^2 S_{11}-S_{33})}{S}\right]\theta - \int f_1 d\theta + f_2 \quad (21)$$

where $f_2$ is only function of $r$. Then, $f_1$ and $f_2$ can be found by the substitution of Eqs. (19) and (21) in (7)

$$f_1 = \frac{C_1(BS_{33}-g_{33}S_{13})}{S_{33}} + D_2 cos\theta + D_3 sin\theta, \quad (22)$$

$$f_2 = rD_1. \quad (23)$$

Here, $D_1$, $D_2$, and $D_3$ are constants of integrations. Therefrom,

$$u(r,\theta) = C_1\left(B - \frac{g_{33}S_{13}}{S_{33}} - \frac{A\left(\frac{r}{r_{in}}\right)^n (n\,S_{13}+S_{33})}{n^2 S_{11}-S_{33}}\right) + \frac{C_2 r(\,S_{13}+S_{33})}{S_{11}-S_{33}} + \frac{C_3 r^{-S}(S\,S_{13}-S_{33})}{S} + \frac{C_4 r^{S}(S\;\;S_{13}+S_{33})}{S} + D_2 cos\theta + D_3 sin\theta, \quad (24)$$

$$v(r,\theta) = (D_1 + C_2\theta)r - D_2 sin\theta + D_3 cos\theta. \quad (25)$$

A remark must however be made on the above formulae. They cannot be applied for $n = 0$, for $n = -1$, or $n = S = \sqrt{S_{33}/S_{11}}$ since they create singularity in the equations (see, e.g., Eq. (18)). Nevertheless, $n = 0$ is not a meaningful value for a grading parameter in piezoelectric materials from an engineering point of view since piezoelectric structures are mostly produced with a combination of minimum two materials or layers (even a unimorph material consists of piezoelectric and elastic layers [39,40]). Hence, this value stays out of the consideration in the present study. On the other hand, the case of $n = -1$ and $n = S$ can be approximated with arbitrary accuracy by choosing some $n$ close to $-1$ (e.g. $-1 \pm 10^{-5}$) and to $S$ (e.g. $S \pm 10^{-5}$) in the numerical calculations, and hence this mathematically singular case is not discussed separately.

It should be also noted that $g_{31}(r)$ should be equal to $g_{31i}$ at the inner surface ($r = r_{in}$) and $g_{31o}$ at the outer surface ($r = r_{out}$) of the bar (see Fig. 1). Then, the constants of A and B in Eq. (4) are determined as

$$A = \frac{g_{31i}-g_{31o}}{1-\left(\frac{r_{out}}{r_{in}}\right)^n}, \quad (26)$$

$$B = g_{31i} - \frac{g_{31i}-g_{31o}}{1-\left(\frac{r_{out}}{r_{in}}\right)^n}. \quad (27)$$

## 4. SOLUTION FOR AN FGP CURVED SENSOR

For a numerical solution of the FGP curved sensor under couple *M* (as illustrated in Fig. 1), 8 unknown constants (i.e. $C_i$ and $D_j$ where $i = 1-5$; $j = 1-3$) should be calculated by using following mechanical and electrical boundary conditions:

$$\phi|_{r=r_{in}} = 0, \quad (28)$$

$$\phi|_{r=r_{out}} = 0, \quad (29)$$

$$\sigma_r|_{r=r_{in}} = 0, \quad (30)$$

$$\sigma_r|_{r=r_{out}} = 0, \quad (31)$$

$$u|_{r=\frac{r_{in}+r_{out}}{2},\theta=\frac{\pi}{2}} = 0, \quad (32)$$

$$v|_{r=\frac{r_{in}+r_{out}}{2},\theta=\frac{\pi}{2}} = 0, \quad (33)$$

$$\frac{\partial u}{\partial \theta}|_{\theta=\frac{\pi}{2}} = 0, \quad (34)$$

$$\int_{r_{in}}^{r_{out}} \sigma_\theta\, r dr = -M. \quad (35)$$

It should be noted that numerical methods are performed to calculate the unknown constants.

## 5. NUMERICAL RESULTS

Firstly, the numerical results for an FGP curved actuator (considering $m = 1$ in Eq. (4)) are compared with the results of Shi's linear FGP actuator model [16] for the verification of the present analytical model. In the illustrations, response variables for the bimorph model of ref. [43] are also presented to provide a general comparison between bimorph and linear FGP actuators. Then the results of the present model for an FGP curved sensor are illustrated to determine the influence of grading parameter $n$. In all numerical results, the inner and outer surface radii are taken $r_{in} = 16\ mm$ and $r_{out} = 17.32\ mm$, respectively, (see Fig. 1) owing to compliance with Shi's [16] and Arslan and Usta's results [43]. In the results, mechanical and electrical coefficients of PZT-4 are used. To provide grading material properties, piezoelectric coefficient $g_{31}$ of the inner surface is taken $g_{31i} = -12 \times 10^{-3}\ m^2/C$ and that of the outer surface is $g_{31o} = 12 \times 10^{-3}\ m^2/C$. The variation of this constant in the radial coordinate $r$ (for $r_{in} \le r \le r_{out}$) for different grading parameters $m$ are presented in Fig. 2. To plot these curves, Eqs. (4), (26), and (27) are used. It should be noted that if $m = 1$, a linear distribution of the coefficient is realized. Moreover, the sign of the parameter m provides the concavity and convexity of the function.

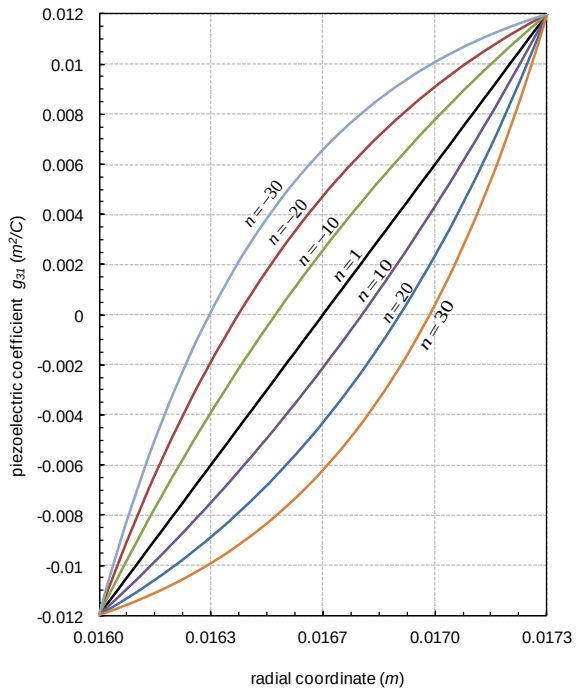


**Figure 2.** Distribution of piezoelectric coefficient $g_{31}$ in the bar for different grading parameter *n*.

The other coefficients of PZT-4 material are assumed to be constant in the whole structure as discussed before. For this treatment, the elastic coefficients are taken as $S_{11} = 1.082 \times 10^{-11}\, m^2/N$, $S_{13} = -2 \times 10^{-12}\, m^2/N$, $S_{33} = 8.28 \times 10^{-12}\, m^2/N$ remaining piezoelectric coefficient is $g_{33} = 2.6 \times 10^{-2}\, m^2/C$, and dielectric coefficient becomes $\zeta_{33} = 86.92 \times 10^{6}$ m/F [47].

### 5.1. Verification of the Model

For the verification of the present model, it is solved for an FGP actuator by considering the linear variation of piezoelectric coefficient $g_{31}$ in radial direction (then $n = 1$ in Eq. (4)). Then, the results and those of linear FGP model in [16] are compared. To obtain response variables for a curved actuator in the present solution, the boundary conditions (29) and (35) should be changed with

$$\phi|_{r=r_{out}} = V_0, \tag{36}$$

$$\int_{r_{in}}^{r_{out}} \sigma_\theta\, r dr = 0, \tag{37}$$

while the other mechanical and electrical conditions (i.e., Eq. (28), Eqs. (30)-(34)) remain the same. Here $V_0$ is an initial electric potential applied to the structure. Now, the linear FGP curved bar is an actuator, not a sensor just because of this boundary condition. The comparison of the response variables for the present model and those for Shi's linear one [16] are presented in Fig. 3. For $V_0 = 100\, V$, the change of radial and circumferential stresses in radial direction and the displacements (at $r = (r_{in} + r_{out})/2 = 16.66\, mm$) in tangential direction are presented in Figs. 3a-3c, respectively. Furthermore, effect of the increasing electric potential $V_0$ (for $0 \le V_0 \le 100\, V$) on the radial and circumferential displacements (at $r = 16.66\, mm$ and $\theta = 0$) is shown in Fig. 3d. In these figures, while solid lines represent the responses of the present model, dots belong to those of Shi's model [16]. As one can see, the comparisons show that the present solution agrees perfectly with that of ref. [16]. In these figures, it is also possible to see the responses for a curved bimorph actuator [43] (dashed lines) to compare FGP and bimorph actuator behaviors under the same electrical load. In the bimorph actuator, the material properties of the inner and outer layers are the same as those of inner and outer surfaces in FGP ($n = 1$) curved actuator.

### 5.2. Results for an FGP Curved Sensor

The piezoelectric bar may behave as a sensor and the production of the electricity is provided, if the couple *M* is applied to the free end of structure (see Fig. 1). The effect of the grading parameter $n$ on the radial stress, circumferential stress, displacements (radial and circumferential components at $\theta = 0$) and electric potential are examined. To do so, $n$ is considered in the range of $-30 \le n < 0$ and $0 < n \le 30$. Results show that the change of grading parameter $n$ does not cause significant differences in stresses and displacements for different $n$ values. The main reason behind this is that the piezoelectric coefficient is just assumed to vary in the radial direction in a grading manner but the elastic coefficients are constant through the bar in the present study. To show the effect of the grading parameter $n$ on the elastic response of the bar, couple *M* is adjusted to $10\, Nm$ and grading parameter $n$ is chosen as $-30$. The results are presented in Figs. 4a-4c for a curved sensor with the dimensions given above. Furthermore, the response variables of a bimorph curved sensor [43] are also presented with dashed lines for comparison. It is noted that inner and outer layer properties of the bimorph structure and the inner and outer surfaces of graded one are the same. As one can see in the figures, the distributions of stresses and displacements are not too different in graded and bimorph materials. Furthermore, it should be emphasized that the maximum radial stress that occurs in the FGP sensor is higher than the bimorph one [43] (see Fig. 4a and Fig. 5a). However, the distribution of the circumferential stress is continuous in FGP but it is discontinuous in the bimorph one at the middle radius (Fig. 4b) since it corresponds to interface radius between the two layers in the bimorph. This situation brings a big advantage to FGP sensor concerning to the failure of the structure. Because, the circumferential stress component in a such sensor is nearly 50 times higher than radial stress. The circumferential component is then dominant one and it is more critical to state the failure of a brittle material such as a ceramic if the maximum principle stress criterion is taken into considered [48]. Moreover, less radial and circumferential displacements take place in the FGP curved sensor with $n = -30$ as seen in Fig. 4c. These results prove the advantage of the grading sensor as far as mechanical behavior is concerned. The influence of different $n$ values is more pronounced in the distribution

of electric potential as one can see in Fig. 4d. This figure presents the changes of electric potentials in the radial coordinate for different $n$ values, i.e. $-30$, 1 and 30, as well as for the bimorph sensor [43] under $M = 10\ Nm$. Even though linear FGP ($n = 1$) and bimorph piezoelectric sensors produce similar electrical potential in the structure, they are significantly different in FGP sensors with $n = 30$ and $n = -30$.

Moreover, to determine effect of grading parameter $n$ on the stresses, displacements and electric potential as well as the change in their maximum values (and also minimum value of electric potential) with different grading parameter $n$ are plotted in Fig. 5. It is noted that $n = 0$ is considered out of the range of the parameters because of the reason discussed in Section 3. In the figures, the corresponding variables for bimorph sensor

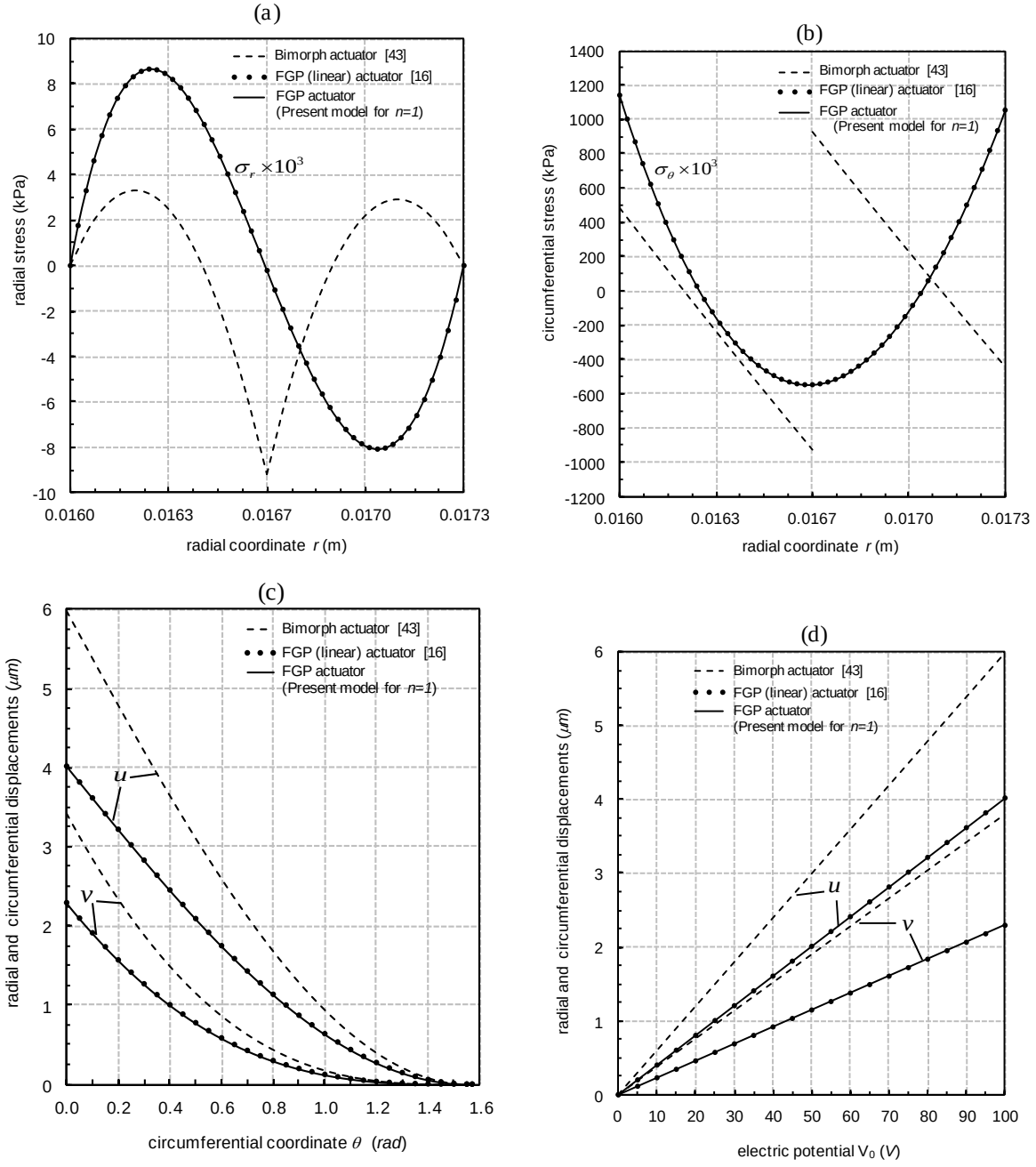


**Figure 3.** Comparison of the response variables in the curved actuators (for $V_0 = 100\ V$) obtained from the present FGP model ($n = 1$), FGP (linear) model [16], and bimorph model [43].

are also marked with a dot. These figures also prove the discussions presented above. It should be also noted that in the FGP sensor (for any $n$ values) maximum radial stress occurs at nearly $r = (r_{in} + r_{out})/2 = 16.66\ mm$, Max. circumferential stress and the radial displacement appear at $r = r_{in} = 16\ mm$ while Max. circumferential displacement occurs at $r = r_{out} = 17.32\ mm$. On the other hand the location of the maximum (and minimum) electric potential values vary in the structure depending on the grading parameter $n$ (see also for Fig. 4d).

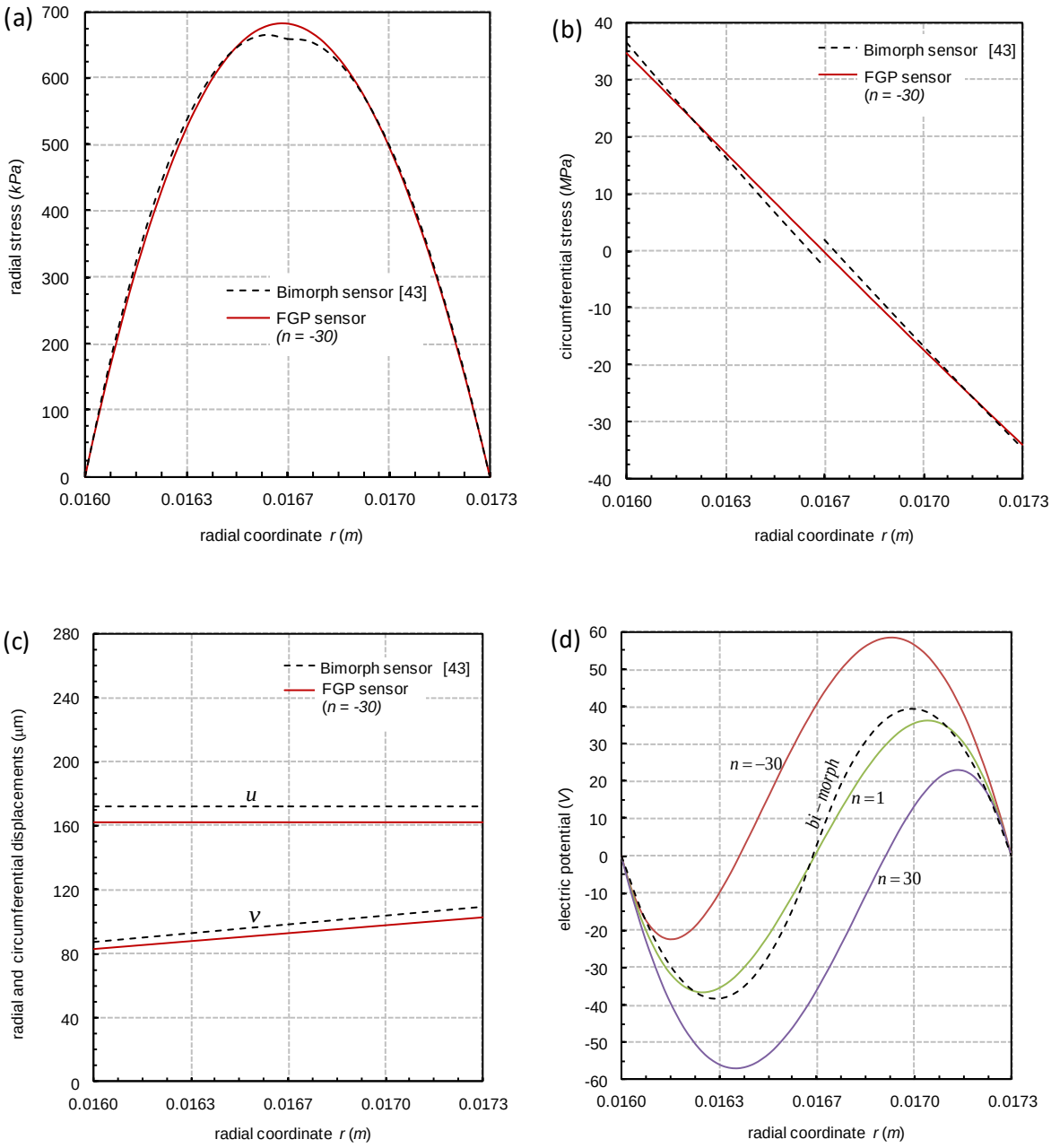


**Figure 4.** Comparison of the response variables in the curved sensors (for $M = 10\ Nm$) obtained from the present FGP model and bimorph model [43].

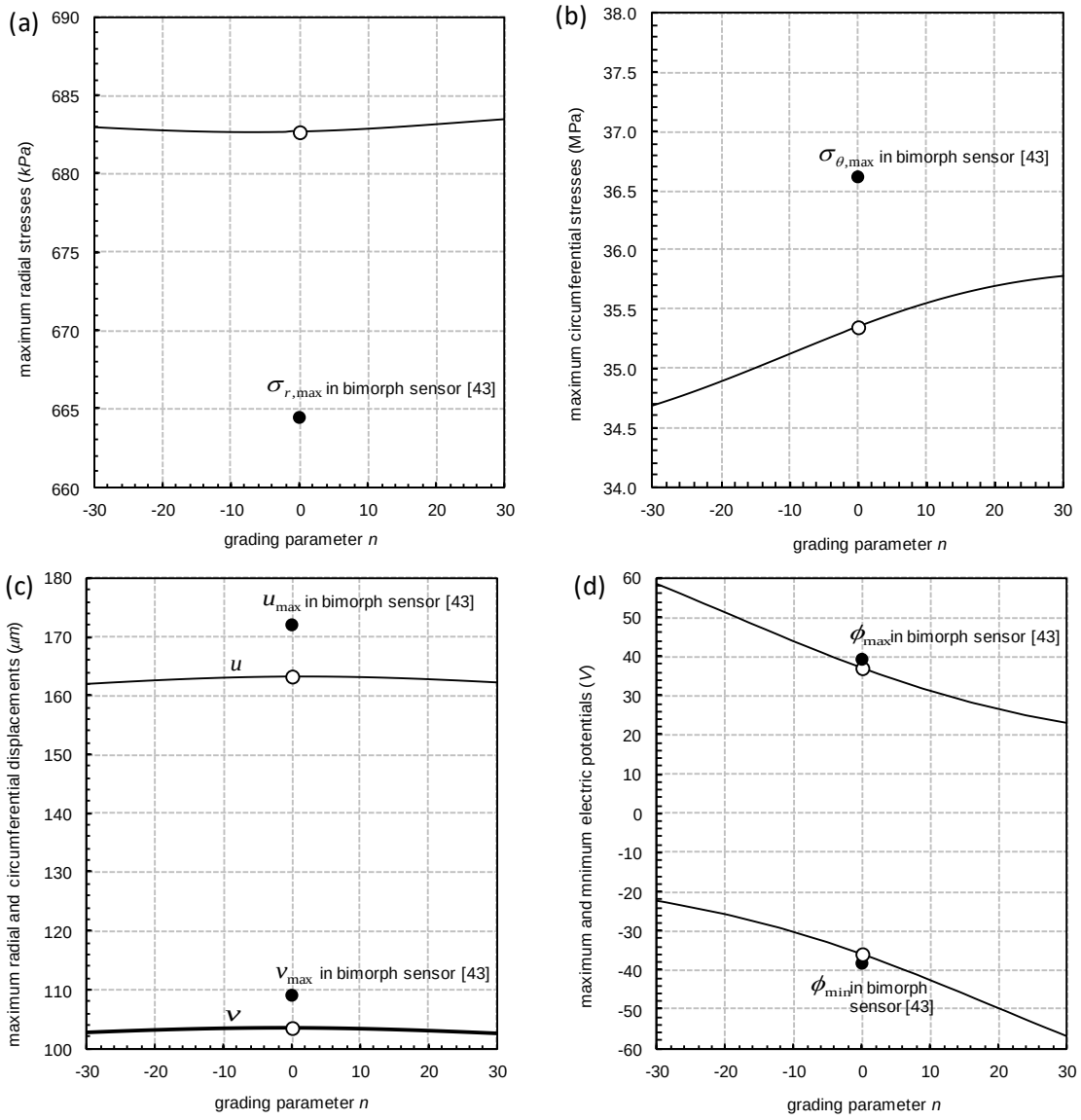


**Figure 5.** Maximum (and minimum) values of the response variables in the FGP sensor with different grading parameters $n$ and for the bimorph sensor [43].

## 6. CONCLUDING REMARKS

A comprehensive mathematical model is developed for a functionally graded piezoelectric (FGP) curved bar being in a closed electrical circuit. It is assumed that piezoelectric coefficient varies in the radial direction according to a nonlinear power law while other material coefficients are assumed to be constant throughout the structure. First, by adjusting the boundary conditions, it is provided that the bar behaves as an actuator, and the reliability of the model is verified by comparing the results with those obtained from linear FGP model [16] in the literature. Then, the boundary conditions are adjusted to obtain stresses, displacements, and electric potential in an FGP curved sensor under a couple, and numerical results are presented.

The influence of the grading parameter on the mechanical and electrical fields is examined and the results are compared with bimorph piezoelectric curved sensors [43]. The results show that the FGP curved sensor has several advantages in terms of the mechanical behavior of the material even though the elastic coefficients are assumed to remain constant in the structure. A continuous distribution of the circumferential stress which is a critical component concerning the failure of the structure are obtained for any grading parameters while distribution of this component is discontinuous on the interface in the bimorph. Moreover, the displacements in the FGP curved sensor are lower than those in the bimorph. Hence, it is considered that FGP curved sensor has more strength than bimorph one due to the fracture and mechanical failure. Effects of the grading parameter also play a considerable role on the distribution and the production of electric potential in the FGP sensor. As the grading parameter is changed, the coordinate and magnitude of the maximum electric

potential produced in the sensor also alter significantly. Therefore, producers and users need to define suitable grading parameters and choose the location of the electrodes in accordance with the application requirements. The present model may be used to observe mechanical and electrical behaviors of any curved actuators and sensors with different dimensions and grading parameters. Hence, the model may serve as a basis for sensor and actuator producers who are interested in piezoelectric materials bonded to structures with curved surfaces.

**REFERENCES**


1. Tadigadapa S. and Mateti K., "Piezoelectric MEMS sensors: state-of-the-art and perspectives", ***Measurement Science and Technology***, 20: 092001, (2009)
2. Tadigadapa S., "Piezoelectric microelectromechanical systems - challenges and opportunities", ***Procedia Engineering***, 5: 468-471, (2010)
3. Sonti V.R. and Jones J.D., "Curved piezoactuator model for active vibration control of cylindrical shells" ***American Institute of Aeronautics and Astronautics Journal***, 34: 1034-1040, (1996)
4. Kielczynski P., Pajewski W. and Szaiewski M., "Piezoelectric sensors for investigations of microstructures" ***Sensors and Actuators A***, 65: 13-18, (1998)
5. Shen M.H., "Analysis of beams containing piezoelectric sensors and actuators", ***Smart Material Structures***, 3: 439-447, (1994)
6. Sirohi J. and Chopra I., "Fundamental Understanding of Piezoelectric Strain Sensors", ***Journal of Intelligent Material Systems and Structures***, 11: 246-257, (2000)
7. Larson P.H. and Vinson J.R., "The use of piezoelectric materials in curved beams and rings Adaptive Structures and Material Systems", ***ASME AD***, 35: 277-285, (1993).
8. Sun D. and Tong L., "Modeling and analysis of curved beams with debonded piezoelectric sensor/actuator patches", ***International Journal of Mechanical Sciences***, 44: 1755-1777, (2002)
9. Ryu D.H. and Wang K.W., "Characterization of surface-bonded piezoelectric actuators on curved beams", ***Smart Materials and Structures***, 11: 377-388, (2002)
10. Sayyaadi H., Rahnama F., Farsangi M.A.A., "Energy harvesting via shallow cylindrical and spherical piezoelectric panels using higher order shear deformation theory", ***Composite Structures***, 147: 155-167, (2016)
11. Zhai J., Zhao G., Shang L., "Integrated design optimization of structure and vibration control with piezoelectric curved shell actuators", ***Journal of Intelligent Material Systems and Structures***, online first, doi:10.1177/1045389X16641203, (2016)
12. Dai L., Wang Y., "Design and simulation of curved sensors of PVDF for fetal heart rate monitoring", ***Symposium on Piezoelectricity, Acoustic Waves, and Device Applications***, 129-132, (2015)
13. Zhang T. and Shi Z.F., "Two-dimensional exact analysis for piezoelectric curved actuators", ***Journal of Micromechanics and Microengineering***, 1: 640-647, (2006)
14. Shi L., Zhang Y., Dong W., "Research on the relationship between the curvature and the sensitivity of curved PVDF sensor", Proc. SPIE 9446, ***Ninth International Symposium on Precision Engineering Measurement and Instrumentation***, 94461Y, doi:10.1117 /12.2180862, (2015)
15. Hauke T., Kouvatov A., Steinhausen R., Seifert W., Beige H., Langhammer H.T. and Abicht H.P., "Bending behavior of functionally gradient materials", ***Ferroelectrics***, 238: 195-202, (2000)
16. Shi Z.F., "Bending behavior of piezoelectric curved actuator", ***Smart Materials and Structures***, 14: 835-842, (2005)
17. Wang Q.M and Cross L.E., "Performance analysis of piezoelectric cantilever bending actuators", ***Ferroelectrics***, 215: 187-213, (1998)
18. Erturk A. and Inman D.J., "An experimentally validated bimorph cantilever model for piezoelectric energy harvesting from base excitations", ***Smart Materials and Structures,*** 18: 1-18, (2009)
19. Smits J.G., Dalke S.I. and Cooney T.K., "The constituent equations of piezoelectric bimorphs", ***Sensors and Actuators A***, 28: 41-61, (1991)
20. Brissaud M., "Modelling of non-symmetric piezoelectric bimorphs", ***Journal of Micromechanics and Microengineering***, 14: 1507-1518, (2004)
21. Brissaud M., Ledren S. and Gonnard P. "Modelling of a cantilever non-symmetric piezoelectric bimorph", ***Journal of Micromechanics and Microengineering***, 13: 832-844, (2003)
22. Shijie Z., Ming C., Zongjun L., Hongtao W., "Size-dependent constituent equations of piezoelectric bimorphs", ***Composite Structures***, 150: 1-7, (2016)
23. Xiang H.J., Shi Z.F., "Static analysis for multi-layered piezoelectric cantilevers", ***International Journal of Solids and Structures***, 45: 113-128, (2008)
24. Weinberg M.S., "Working equations for piezoelectric actuators and sensors", ***Journal of Microelectromechanical Systems***, 8: 529-533, (1999)
25. Shi Z.F., Xiang H.J. and Spencer Jr.B.F., "Exact analysis of multi-layer piezoelectric/composite cantilevers", ***Smart Materials and Structures***, 15: 1447-1458, (2006)
26. Vel S.S. and Batra R.C., "Exact solution for the cylindrical bending of laminated plates with embedded piezoelectric shear actuators", ***Smart Materials and Structures***, 10: 240-251, (2001)
27. Shi Z.F. and Chen Y., "Functionally graded piezoelectric cantilever beam under load", ***Archive of Applied Mechanics***, 74: 237-247, (2004)
28. Yu T. and Zhong Z., "Bending analysis of a functionally graded piezoelectric cantilever beam", ***Science in China Series G: Physics, Mechanics & Astronomy***, 50: 97-108, (2007)
29. Chen Y. and Shi Z.F., "Exact Solutions of Functionally Gradient Piezothermoelastic Cantilevers and Parameter Identification", ***Journal of Intelligent Material Systems and Structures***, 16: 531-539, (2005)
30. Huang D.J., Ding H.J. and Chen W.Q., "Piezoelasticity solutions for functionally graded piezoelectric beams", ***Smart Materials and Structures***, 16: 687-695, (2007)

31. Liu T. and Shi Z.F., "Bending behavior of functionally gradient piezoelectric cantilever", ***Ferroelectrics***, 308: 43-51, (2004)
32. Taya M., Almajid A.A., Dunn M. and Takahashi H., "Design of bimorph piezo-composite actuators with functionally graded microstructure", **Sensors and Actuators A: Physical**, 107: 248-260, (2003)
33. Shi Z. F. and Zhang T., "Bending analysis of a piezoelectric curved actuator with a generally graded property for the piezoelectric parameter", ***Smart Materials and Structures***, 17: 045018, (2008)
34. Li Y.S., Pan E., "Static bending and free vibration of a functionally graded piezoelectric microplate based on the modified couple-stress theory", ***International Journal of Engineering Science***, 97: 40-59, (2015)
35. Komijani M., Reddy J.N., Eslami M.R., "Nonlinear analysis of microstructure-dependent functionally graded piezoelectric material actuators", ***Journal of the Mechanics and Physics of Solids***, 63: 214-227, (2014)
36. Arslan E. and Eraslan A.N., "Bending of graded curved bars at elastic limits and beyond", ***International Journal of Solids and Structures***, 50: 806-814, (2013)
37. Arslan E. and Mack W., "Shrink fit with solid inclusion and functionally graded hub", ***Composite Structures***, 121: 217-224, (2015)
38. Birman V. and Byrd L.W., "Modeling and analysis of functionally graded materials and structures", ***Applied Mechanics Reviews***, 60: 195-216, (2007)
39. Anton S.R. and Sodano H.A., "A review of power harvesting using piezoelectric materials (2003-2006)", ***Smart Materials and Structures***, 16: R1-R21, (2007)
40. Kuang Y.D., Li G.Q., Chen C.Y. and Min Q., "The static responses and displacement control of circular curved beams with piezoelectric actuators", ***Smart Materials and Structures***, 16: 1016-1024, (2007)
41. Zhou Y., Nyberg T.R., Xiong G., Zhou H., "Precise deflection analysis of laminated piezoelectric curved beam", ***Journal of Intelligent Material Systems and Structures***, online first, doi:10.1177/1045389X15624797, (2016)
42. Su Z., Jin G., Ye T., "Vibration analysis and transient response of a functionally graded piezoelectric curved beam with general boundary conditions", Smart Materials and Structures, 25: 065003, (2016)
43. Arslan E. and Usta R., "Mechanical and electrical fields of piezoelectric curved sensors", ***Archives of Mechanics***, 66: 329-342, (2014)
44. Timoshenko S.P. and Goodier J.N., "Theory of Elasticity", ***McGraw-Hill***, (1970)
45. Arslan E. and Eraslan A.N., "Analytical solution to the bending of a nonlinearly hardening wide curved bar", ***Acta Mechanica***, 210: 71-84, (2010)
46. Kielczynski P. and Pajewski W., "Influence of a layered polarization of piezoelectric ceramics on shear-horizontal surface-wave propagation", ***Applied Physics B***, 48: 383-388, (1989)
47. Ruan X., Danforth S.C., Safari A. and Choua T.W., "Saint-Venant end effects in piezoceramic materials", ***International Journal of Solids and Structures***, 37: 2625-2637, (2000)
48. Mendelson A., "Plasticity: Theory and Application", ***Macmillan***, New York, (1968)